Malaysian Journal of Chemistry, 2023, Vol. 25(5), 1-12
(Special Issue: *4th International Symposium on Multidisciplinary Science 2022*)

In Silico Studies of Carotenoids from *Chlorella* sp. Microalgae against S-Shaped Amyloid Beta Fibril

Norzalina Zakaria[1,2], Nur Juliyana Bella Hanifah[1], Siti Nor Ani Azaman[3] and Nur Hana Faujan[2,3]*

[1]Department of Chemistry, Faculty of Science, Universiti Putra Malaysia, 43400 UPM Serdang, Selangor Darul Ehsan, Malaysia
[2]Integrated Chemical Biophysics Research, Faculty of Science, Universiti Putra Malaysia, 43400 UPM Serdang, Selangor Darul Ehsan, Malaysia
[3]Center of Foundation Studies for Agricultural Science, Universiti Putra Malaysia, 43400 UPM Serdang, Selangor Darul Ehsan, Malaysia
*Corresponding author (e-mail: nurhana@upm.edu.my)

Chlorella sp. is green freshwater microalgae have drawn great attention as a promising sustainable source of lipids and carotenoids. As neuroprotective natural products, carotenoids have shown promising preventive activity, as well as helping in slowing down Alzheimer's disease (AD) progression. However, the detailed information on the inhibition mechanism of amyloid beta (Aβ) fibril, one of the hallmarks of AD, by carotenoid compounds is poorly discussed in both experimental and computational studies. Thus, in this study, molecular docking simulations were performed to investigate the binding interactions between nine carotenoid compounds derived from *Chlorella* sp. against full sequence $A\beta_{42}$ fibril. The results reveal that the binding energies ranged from -5.3 to -6.5 kcal/mol with binding interactions were dominated by hydrophobic interactions via π-alkyl, and only two carotenoid compounds, fucoxanthin and zeaxanthin, formed hydrogen bonds. In comparison, donepezil showed binding energy of -6.7 kcal/mol and interacted with $A\beta_{42}$ residues through a hydrogen bond and hydrophobic interaction that involves alkyl, π-alkyl, π-sigma and π-π T-shape interactions. Our result showed that donepezil, fucoxanthin and zeaxanthin compounds disrupted the $A\beta_{42}$ fibril by disaggregation pathway, which primarily interacted with residues within the hydrophobic (Phe19, Phe20, Val24, Ala30, and Ile32) and N-terminal (Tyr10, Val12, His13, and His14) regions. This study provides theoretical insights into the inhibitory mechanism of antioxidant compounds against Aβ fibril, which is beneficial for AD drug design.

Keywords: Alzheimer's disease; Amyloid beta fibril; *Chlorella* sp.; Carotenoids; Molecular docking

Received: July 2022; Accepted: January 2023

Alzheimer's disease (AD) is one of the most common neurodegenerative diseases characterized by impaired cognitive abilities and memory loss [1], affecting more than 34 million people worldwide [2,3]. Financially it is very costly, posing a great burden to society. AD is postulated to be caused by an abnormal accumulation of amyloid beta (Aβ) peptides consisting of 40 and 42 amino acids, derived by β and γ-secretase cleavage from Aβ precursor protein (APP) [4,5]. Both $A\beta_{40}$ and $A\beta_{42}$ are soluble helical peptides that undergo a conformational transition from α-helix to β-sheet structures and eventually form β-sheet-enriched fibril structures [6]. Previous studies of Aβ toxicity revealed that fibrillar Aβ could directly kill neurons or initiate a cascade of events leading to neuronal cell death [7-9]. The lack of cures for Alzheimer's disease poses a major challenge because many available AD drugs only reduce the symptoms of dementia and are not capable of preventing the progression of the disease, and do not halt the slow deterioration of the brain [10,11]. Current treatments, including donepezil, rivastigmine and galantamine, are prescribed for mild to moderate AD to manage and control the symptoms of the disease, but suffer some limitations such as toxicity, cell cycle specificity, and development of drug resistance [10]. Therefore, research on searching for a cure for AD has been extensively performed, and one of the prominent mechanisms proposed involving Aβ is by preventing the β-sheet-enriched fibril formation or by inducing degradation of already formed β-sheet-based aggregates [11].

A *Chlorella* sp. is a group of eukaryotic green microalgae found in fresh or salty water and on surfaces of different soil types [12,13]. These microalgae can grow with little water, a small number of nutrients, carbon dioxide, and sunlight due to their extremely simple structure [14,15]. Due to their richness of high-value chemical compounds such as carotenoids (astaxanthin, lutein, β-carotene, violaxanthin, and

†Paper presented at the 4th International Symposium on Multidisciplinary Science 2022 (SMS 2022)

zeaxanthin), antioxidants, vitamins, polysaccharides, proteins, peptides, fatty acids, and others [14], *Chlorella* has been applied in various industries such as food, pharmaceutical, cosmetic, and others [16]. Over the last decade, carotenoids, a family of yellow, orange, and red pigments have emerged as potential compounds for AD treatment [17-19]. Carotenoids belong to a terpenoid class with a characteristic conjugated polyene chain composed of eight units of C5 isoprenoid. Based on their chemical structures, carotenoids are categorized into two main groups: carotene, which consists of only carbon and hydrogen atoms, and xanthophyll, which consists of carbon and hydrogen with oxygen in the form of epoxy, carboxy, keto, hydroxy, and methoxy positions. Most carotenoids are lipophilic and can cross the blood-brain barrier [20].

Several studies have demonstrated that carotenoids can potentially reduce the risk of AD by inhibiting aggregation and destabilizing Aβ fibrils [20-24, 44]. Katayama and coworkers demonstrated that lutein had the strongest inhibitory effect on Aβ fibril formation compared to zeaxanthin, β-cryptoxanthin, β-carotene, and α-carotene through an in-vitro study [20]. Lakey-Beitia and coworkers reported a similar result through an in-silico molecular docking study highlighting that lutein had the highest binding affinity compared to astaxanthin, bixin, cryptocapsin, and fucoxanthin when in complex with different types of Aβ fibril polymorphs obtained from RCSB Protein Data Bank (PDB code: 2BEG, 2MXU, 2NAO, 2M4J) [21]. The number and position of hydroxyl groups, together with the hydrophobic chain of polyene units, play an important role in inhibiting Aβ aggregation through forming hydrogen bonds and hydrophobic interactions with Aβ fibril residues [22].

Carotenoids are potent natural antioxidants, and most of the studies demonstrated that carotenoids reduced AD through the neuroinflammation pathways [25] by suppressing the interleukin-1β (IL-1β) and tumour necrosis factor-alpha (TNF- α) action [26] as well as inhibiting the nuclear translocation of kappaB (NfkB) and reactive oxygen species (ROS) production [27]. The investigations of the effects of carotenoids directly on Aβ plaques formation or disruption are very limited in both experimental and computational studies. Furthermore, Aβ fibrils are well known to have a variety of polymorphisms [28], and different polymorph structures will have different inhibition mechanisms. However, most published literature only focused on inhibiting U-shaped Aβ fibril [29-31, 47-48].

Recent studies have reported that the aggregation and fibrillation of $A\beta_{42}$ peptide also result in the formation of S-shaped $A\beta_{42}$ fibril, which is more stable and toxic as compared to U-shaped Aβ fibril [32]. Since the S-shaped $A\beta_{42}$ fibril imposes more toxicity to the human brain and the inhibition study of carotenoids on this S-shaped $A\beta_{42}$ fibril conformation is very limited. Thus, molecular docking simulations were utilized in the present study to investigate the inhibition mechanism of nine carotenoid compounds derived from *Chlorella* sp. against a complete sequence of S-shaped $A\beta_{42}$ fibril.

METHODOLOGY

Preparation of Initial Structures

The three-dimensional (3D) NMR structure of $A\beta_{42}$ fibril, which consists of ten conformations, was obtained from RCSB Protein Data Bank (PDB) with a corresponding PDB code of 2NAO [33]. The first conformation was chosen, and the other nine conformations were removed using AutoDockTools (ADT) 1.5.6 [34]. Only chains A, B, and C were chosen (Figure 1) to be docked with nine carotenoid compounds (Figure 2) and donepezil (PubChem CID: 3152) as a positive control. The remaining chains (D, E, and F) were removed using Discovery Studio Visualizer (DSV) 19.1 [35]. Meanwhile, the 3D structures of nine carotenoid and donepezil conformers were downloaded from the NCBI PubChem database [36] in SDF format. These structures were then optimized using a Dreiding-like force field [37] and converted into PDB format using DSV 19.1.

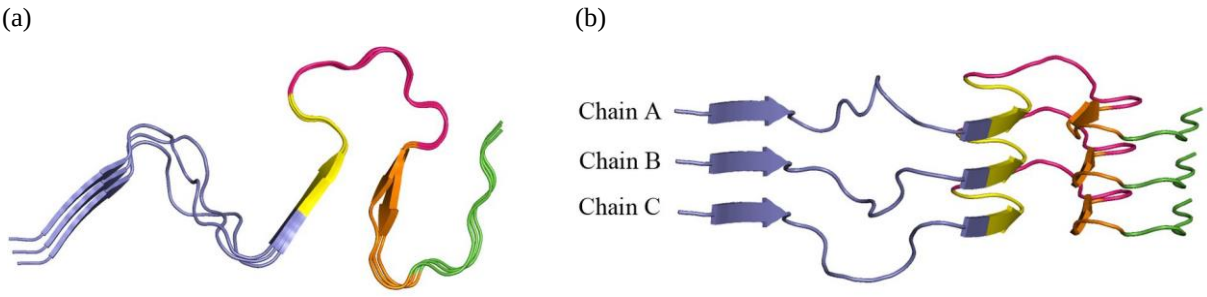

Figure 1. 3D cartoon representations of $A\beta_{42}$ fibril (PDB code: 2NAO) are shown in (a) the top and (b) the front view. The N-terminal: D1-K16 and turn: E22-G29 are shown in slate blue and hot pink, respectively. The hydrophobic regions, central hydrophobic core (CHC): L17-A21, second hydrophobic core (SHC): A30-M35, and C-terminal: V36-A42, are shown in yellow, orange, and green, respectively.

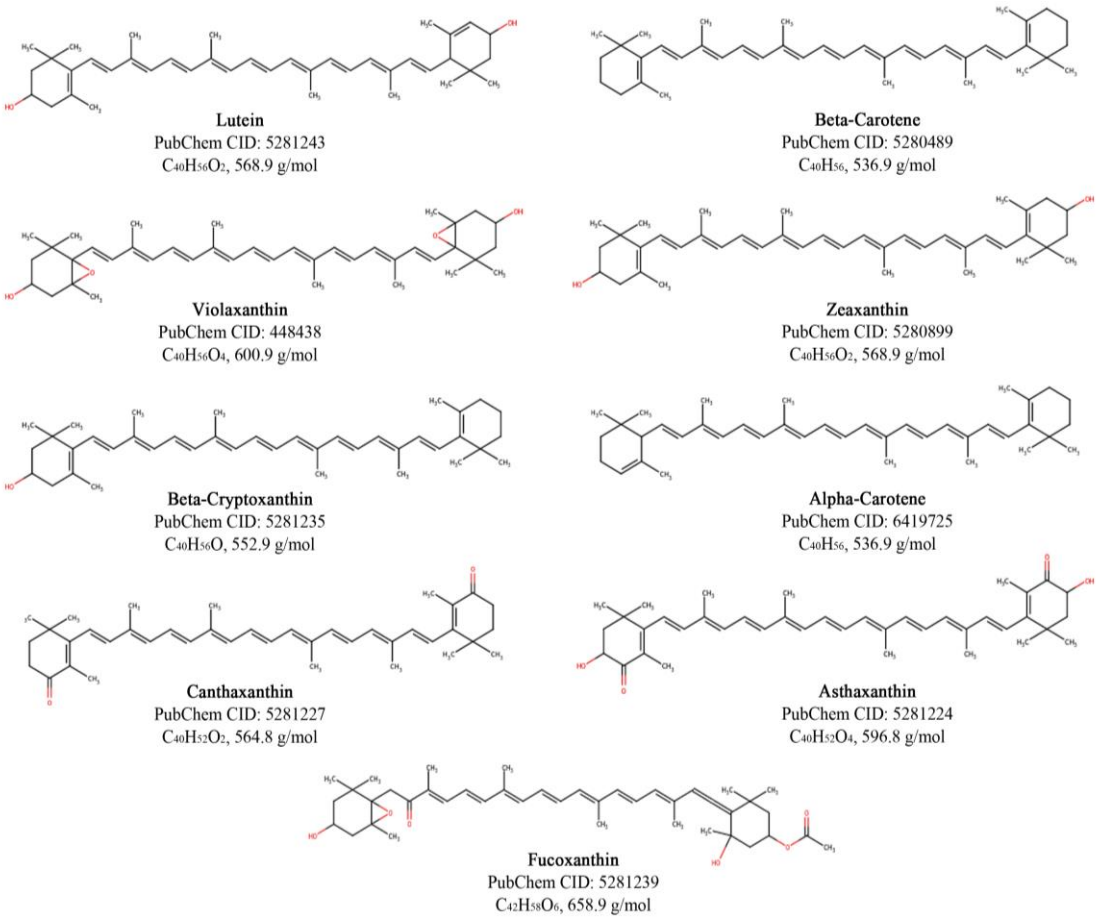

Figure 2. Chemical structures of carotenoid compounds with their respective PubChem CID, molecular formula, and molecular weight. These structures were sketched and generated using the SwissADME server [38].

Preparation of Input (PDBQT) Files and Grid Box Parameter

Before performing molecular docking, both protein and ligand structures in PDB format must be converted into PDBQT format using ADT 1.5.6. In this step, missing hydrogen atoms were added, and non-polar hydrogen atoms were merged, followed by the addition of Kollman and Gasteiger charge to protein and ligands, respectively. Next, because the binding site of $A\beta_{42}$ fibril was not a priori known, thus a large grid box with a dimension of 126×114×124 was created and enclosed the fibril with default spacing. This grid box was large enough to allow the carotenoid and donepezil ligands to translate and rotate around the fibril surface.

Molecular Docking Simulations

AutoDock Vina 1.1.2 [39] was employed in the molecular docking process to determine the binding energy and interactions between carotenoid ligands and $A\beta_{42}$ fibril. The Iterated Local Search global optimizer algorithm [40] was used for each ligand to perform default docking runs. The protein was set as rigid, and the ligand was set as flexible. The binding energy for the interaction between each carotenoid and $A\beta_{42}$ fibril was eventually calculated, and the best conformation was selected based on its lowest free binding energy. For analysis, PyMOL 2.3.0 [41] and DSV 19.1 were used to visualize the 3D structure of complexes and to generate two-dimensional (2D) representations of the protein-ligand interactions.

RESULTS AND DISCUSSIONS

In this study, molecular docking simulations were performed using AutoDock Vina 1.1.2 to predict the binding affinity and interactions between $A\beta_{42}$ fibril and nine carotenoid compounds, compared with the positive control, donepezil. Table 1 shows that the binding energies of donepezil and nine carotenoids derived from *Chlorella* sp. ranged from -5.3 to -6.7 kcal/mol.

As shown in Figure 3a, we identified four binding sites, A, B, C, and D. Site A was the most plausible binding site on $A\beta_{42}$ fibril since it accommodated the largest docked carotenoid compounds (lutein, violaxanthin, zeaxanthin, beta-carotene, and fucoxanthin) with the top-ranking binding energies between -5.8 and -6.5 kcal/mol. Interestingly, lutein, violaxanthin, zeaxanthin, beta-carotene, and fucoxanthin exhibited a similar binding

site on $A\beta_{42}$ fibril with donepezil. Donepezil had been found on $A\beta_{42}$ fibril at site A with the lowest binding energy of -6.7 kcal/mol. This site comprised the last part the N-terminal (H13-K16), CHC (L17-F20), turn (V24, S26, N27), and SHC (A30, I32, L34) regions of chain A. The second site, B, accommodated a beta-cryptoxanthin with a binding energy of -6.2 kcal/mol. Residues in this site involved the last part of the N-terminal (V12-H14), CHC (L17-A21), and the early part of turn (E22-G25) regions of chain C. Next, the third site, C, was located vertically in the first interior of $A\beta_{42}$ fibril. This site comprised the N-terminal residues (H6-Y10) of chains A, B, and C. It accommodated alpha-carotene and astaxanthin, with both having a similar binding energy of -5.8 kcal/mol. The fourth site, D, comprised the N-terminal residues (D1-F5) of chain C, accommodated half of the canthaxanthin, and the other half was located on- and overlapped with the bottom part of site C, with the total highest binding energy of -5.3 kcal/mol.

Table 1. Docking results of donepezil and nine carotenoid compounds with $A\beta_{42}$ fibril.

Ligand	Binding Energy (kcal/mol)	Interactions			
		Hydrogen Bond	Hydrophobic		
			alkyl	π-alkyl	π-sigma
Donepezil	-6.7	Gly33A	Leu17A, Ile32A, Leu34A	Val24A	Phe19A, Ile32A
Lutein	-6.5		Leu17A, 3 Val24A Ala30A, Ile32A	His13A, 3 Phe19A, 3 Phe20A	
Violaxanthin	-6.4		3 Val24A, Ala30A, Ile32A	2 His13A, 5 Phe19A, 3 Phe20A	
Fucoxanthin	-6.3	Gln15A	2 Leu17A, Val24A, 3 Ile32A, Leu34A, Leu34B	2 His14A, 3 Phe19A, Phe20A	
Beta-Cryptoxanthin	-6.2		2 Val12C, 5 Val18C, Val24C	2 His13C, His14C, 2 Phe20C	
Beta-Carotene	-6.2		Leu17A, 2 Ile32A, 2 Leu34A	4 Phe19A	
Zeaxanthin	-5.8	Ser26A	Val24A, 2 Ala30A	His13A, 3 Phe19A, 2 Phe20A	
Alpha-Carotene	-5.8		2 Val12A	Phe4A, His6A, Tyr10A, 3 His6B, 2 His13B, 2 Tyr10C, 2 His13C	2 His6A, His13C
Astaxanthin	-5.8			Phe4A, His13B, 2 Tyr10C, 2 His13C	His6A, His6B
Canthaxanthin	-5.3			His14B, Phe4C, 3 Tyr10C, 2 His13C	

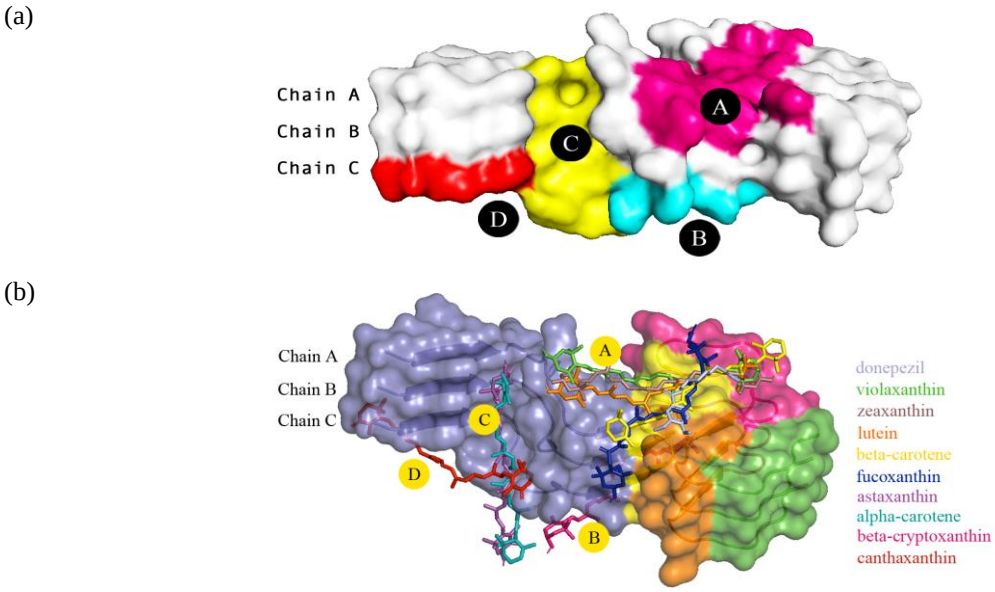

Figure 3. (a) 3D representations of the binding sites, A, B, C, and D, and (b) the best poses of nine carotenoids and donepezil at different binding sites of $A\beta_{42}$ fibril.

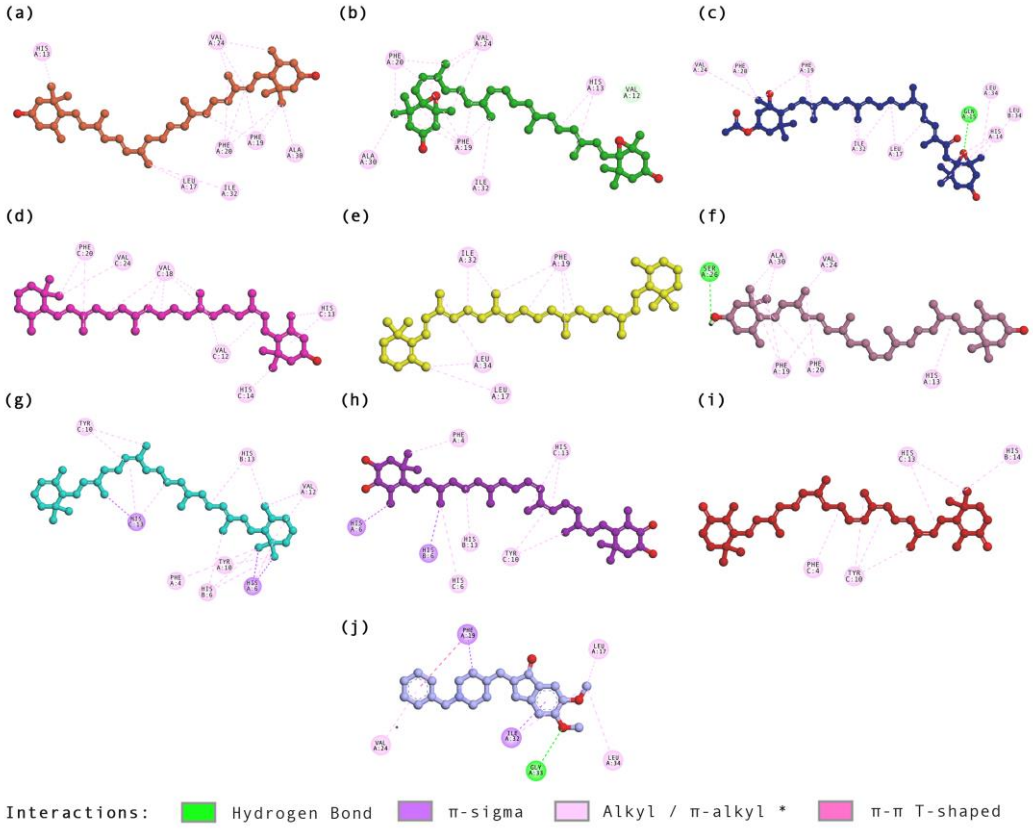

Figure 4. 2D interaction maps between $A\beta_{42}$ against (a) lutein, (b) violaxanthin, (c) fucoxanthin, (d) beta-cryptoxanthin, (e) beta-carotene, (f) zeaxanthin, (g) alpha-carotene, (h) astaxanthin, (i) canthaxanthin, and (j) donepezil.

Figure 4 shows that the interactions between $A\beta_{42}$ fibril with nine carotenoid compounds were dominated by hydrophobic interactions, which consist of three types: 1) alkyl interactions that involved residues with hydrocarbon alkyl groups side chain, alanine (Ala30), valine (Val12, Val18, Val24), leucine (Leu17, Leu34), and isoleucine (Ile32); 2) π-alkyl interactions that involved residues with aromatic groups side chain, tyrosine (Tyr10), histidine (His6, His13, His14), and phenylalanine (Phe4, Phe19, Phe20) and 3) π-sigma interactions that involved only histidine (His6, His13) residues. Furthermore, only

two carotenoids, fucoxanthin and zeaxanthin, were observed to form hydrogen bonds with Gln15A (2.22 Å) and Ser26A (2.83 Å) of $A\beta_{42}$ fibril, respectively. We compared the binding modes of donepezil and carotenoids within the active site of $A\beta_{42}$ fibril. The donepezil also displayed hydrophobic contacts with $A\beta_{42}$ fibril by forming the: 1) alkyl interaction with Leu17A, Leu34A, Ile32; 2) π-alkyl interaction with Val24; and 3) π-sigma interaction with Phe19A, Ile32. Similar to fucoxanthin and zeaxanthin, donepezil also formed the hydrogen bond, however, with a different residue of $A\beta_{42}$ fibril, Gly33A (2.86 Å).

The domination of hydrophobic interaction is due to carotenoids' chemical structure and position on $A\beta_{42}$ fibril. Carotenoids are hydrophobic antioxidants [42] which comprise a long-straight-hydrophobic polyene main chain with terminal ionone rings. In this study, most carotenoids deposited on CHC and SHC regions, and the methyl groups attached to the main chain and terminal rings of carotenoids interacted with hydrophobic residues of $A\beta_{42}$ fibril, forming alkyl and π-alkyl interactions.

In the protein-ligand study, the intermolecular hydrogen bond is formed by the participation of nitrogen (N) and oxygen (O) atoms of the backbone and polar side chain (Arg, Asn, Asp, Gln, Glu, His, Lys, Ser, Thr, Trp, Tyr) of protein with N, O, sulphur (S), and halogen atoms from the ligand [43]. Thus, α- and β-carotene consisting of only carbon and hydrogen atoms, are incapable of forming hydrogen bonds. Figure 5 shows the polar residues (pink-coloured carbon atoms) of chain A, which may interact with donepezil, lutein, and zeaxanthin via hydrogen bonds due to the positions of these three ligands were near polar residues, and they possess the O atoms in their structure. However, based on Figure 5, it can be seen that only donepezil and zeaxanthin formed the hydrogen bonds with Gly33A (2.86 Å) and Ser26A (2.83 Å), respectively, due to their hydrogen bond distances which are in the range of typical hydrogen bond distance, 2.5 to 3.4 Å [43]. These results indicate that the chemical structure, position, and orientation of a ligand on the receptor play an important role in the formation of the hydrogen bond.

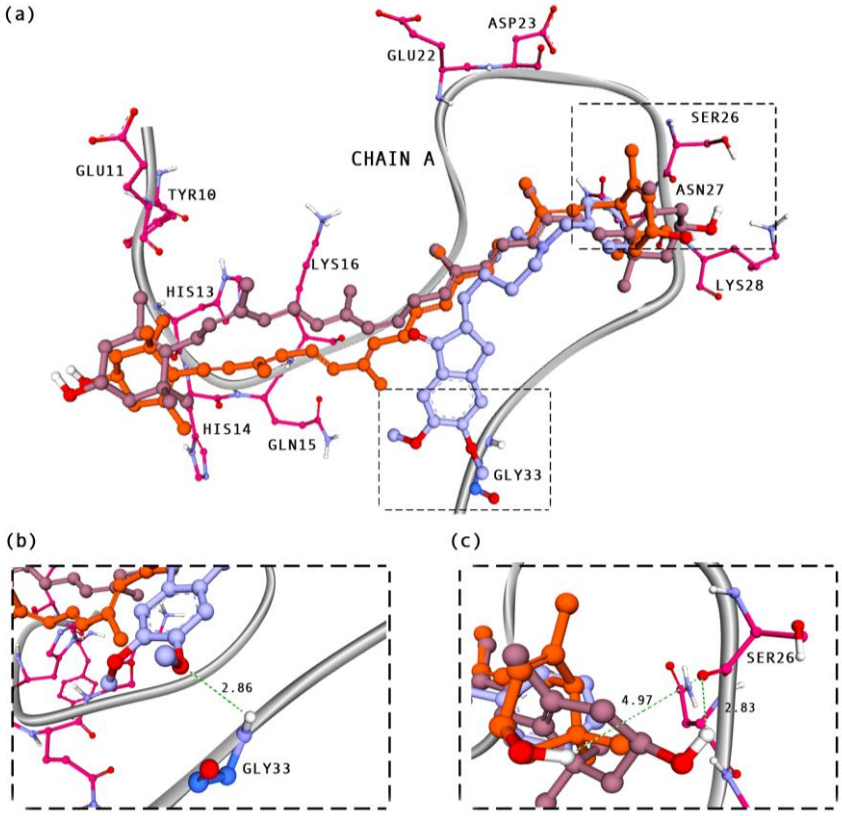

Figure 5. (a) The 3D poses of donepezil (slate blue), lutein (orange), and zeaxanthin (mauve) on chain A of $A\beta_{42}$ fibril, (b) the distance between hydrogen acceptor of donepezil and hydrogen donor of Gly33A, and (c) the distance between hydrogen donor of lutein and zeaxanthin with hydrogen acceptor of Ser26A. The polar side chain residues are shown in pink-coloured carbon atoms.

Table 2. Binding interactions of carotenoid compounds with $A\beta_{42}$ residues classified by regions.

Carotenoids	$A\beta_{42}$ regions			
	N-terminal (D1-K16)	**CHC (L17-A21)**	**Turn (E22-G29)**	**SHR (A30-M35)**
Donepezil		Leu17A, 2 Phe19A	Val24A	2 Ile32A, Gly33A, Leu34A
Lutein	His13A	Leu17A, 3 Phe19A, 3 Phe20A	3 Val24A	Ala30A, Ile32A
Violaxanthin	2 His13A	5 Phe19A, 3 Phe20A	3 Val24A	Ala30A, Ile32A
Fucoxanthin	2 His14A, Gln15A	2 Leu17A, 3 Phe19A, Phe20A	Val24A	3 Ile32A, Leu34A, Leu34B
Beta-Cryptoxanthin	2 Val12C, 2 His13C, His14C	5 Val18C, 2 Phe20C	Val24C	
Beta-Carotene		Leu17A, 4 Phe19A		2 Ile32A, 2 Leu34A
Zeaxanthin	His13A	3 Phe19A, 2 Phe20A	Val24A, Ser26A	2 Ala30A
Alpha-Carotene	Phe4A, 3 His6A, Tyr10A, 2 Val12A, 3 His6B, 2 His13B, 2 Tyr10C, 3 His13C			
Astaxanthin	Phe4A, His6A, His6B, His13B, 2 Tyr10C, 2 His13C			
Canthaxanthin	His14B, Phe4C, 3 Tyr10C, 2 His13C			

Previous computational studies focused on the U-shaped $A\beta_{17-42}$ fibril (PDB code: 2BEG) reported that small molecules [29-31] as well as carotenoid compounds [21] primarily interacted with salt-bridge (A21-K28) and secondarily interacted with SHC (A30-M35), and C-terminal (V36-A42) residues. In this study, donepezil, lutein, violaxanthin, fucoxanthin and zeaxanthin have been shown to interact with S-shaped $A\beta_{42}$ fibril at CHC (L17-A21), turn (E22-G29) and SHR (A30-M35) regions. However, alpha-carotene, astaxanthin, and canthaxanthin interacted primarily with N-terminal (D1-K16) residues (Table 2), which is crucial for aggregation through the interactions with metals. The preferential binding of these three carotenoid compounds to the N-terminal region was likely due to the presence of aromatic residues (Phe4, His6, Tyr10, His13) and the ability of the compounds to fill the space in the pocket [46].

Disagreement in the observed primary binding site of these three carotenoids compared to the previous study are most likely due to differences in the Aβ polymorph used in each study. The U-shaped $A\beta_{17-42}$ fibril 2BEG does not consist of the N-terminal pocket that is present in the S-shaped $A\beta_{42}$ fibril 2NAO used in the current study. The 2BEG structure consists of the first (L17−S26) and second (I31−A_{42}) β-strand connected by a turn region (N27−A30). A small molecule such as morin has been reported, penetrating the interior of the hydrophobic core and disrupting the D23-A28 salt bridges by interfering with native backbone hydrogen bonds and eventually leading to the destabilization of $A\beta_{17-42}$ fibril [47]. Fan and coworkers also reported that this interior hydrophobic groove was the most plausible site with the lowest binding energy when forming a complex with wgx-50 ligand, a compound extracted from Sichuan pepper *(Zanthoxylum bungeanum)* [48].

The intramolecular network interactions in U-shaped $A\beta_{17-42}$ fibril 2BEG involving the interior hydrophobic groove are shown in Figure 6a. In contrast, two hydrophobic pockets formed from the intramolecular interactions between Leu17-Ile32, Phe19-Phe20, Phe19-Ala30, Phe19-Ile32, Phe20-Val24, Phe20-Ala30, and Ile31-Val39 in S-shaped $A\beta_{1-42}$ fibril 2NAO (Figure 6b). Instead of having a traditional D23-K28 salt bridge, it has been reported that $A\beta_{42}$ fibril formed

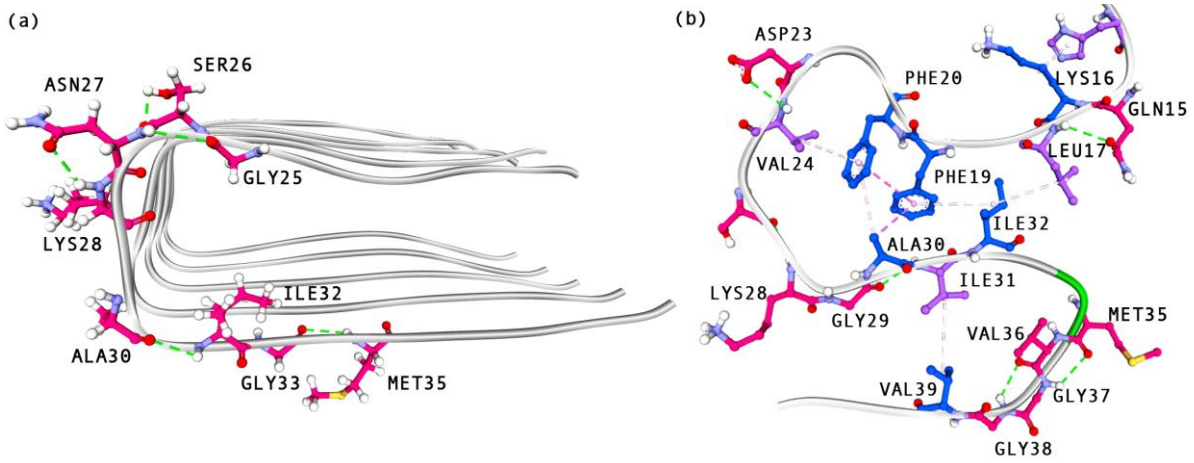

Figure 6. 3D representations of intramolecular network interactions in chain A of (a) U-shaped $A\beta_{17-42}$ fibril 2BEG and (b) S-shaped $A\beta_{42}$ fibril 2NAO. The residues that formed hydrogen bonds, hydrophobic contacts, and the combination of both interactions, are shown in pink, blue and purple, respectively.

Table 3. Intramolecular interaction networks in chain A of $A\beta_{42}$ fibril.

Residue	Hydrogen Bond	Hydrophobic Interactions			
		alkyl	π-alkyl	π-sigma	π-π T-shaped
D1-L17	His6-Ser8, Gly9-Glu11, Glu11-His13, Gln15-Leu17		Ala2-Phe4, His13-Lys16		
L17-A42	Asp23-Val24, Ser26-Lys28, Gly29-Ile31, Met35-Gly37, Val36-Gly38	Leu17-Ile32, Ile31-Val39	Phe19-Ile32, Phe20-Val24, Phe20-Ala30	Phe19-Ala30	Phe19-Phe20

the salt-bridge interactions between Lys28 and Ala42 [49-50]. The formation of two hydrophobic pockets and the salt bridge plays an important role in maintaining the S-shaped conformational structure of $A\beta_{42}$ fibril.

In this study, S-shaped $A\beta_{42}$ fibril 2NAO was used as a receptor, and the mechanisms involved in the aggregation and disaggregation pathway of Aβ fibril are quite different compared to the previous studies, which mostly used U-shaped $A\beta_{17-42}$ fibril 2BEG. S-shaped $A\beta_{42}$ fibril 2NAO displays triple parallel-β-sheet segments with D1–H14 residues that are partially ordered and not entirely rigid, whereas Q15–A42 residues form a double-horseshoe–cross– a β-sheet entity with maximally buried hydrophobic side chains in the two distinct hydrophobic cores, one containing residues Leu17, Phe19, Phe20, Val24, Ala30, and Ile32, and the other containing Ile31, Val36, Val39, and Ile41 [49-50]. The intramolecular interaction networks in chain A of $A\beta_{42}$ fibril are shown in Table 3.

Our docking results highlight that donepezil and five carotenoid compounds (lutein, violaxanthin, fucoxanthin, beta-carotene, and zeaxanthin) interacted with K16-F20 residues of the binding sites A, which are responsible for the initiation of aggregation [21]. U-shaped Aβ fibril (PDB ID: 2BEG) bears two amyloidic regions, the first sequence at K16–A21 and the second sequence at I32–V36 [51]. These carotenoids showed a similar binding pattern with the first sequence of the amyloidic region of 2BEG. Besides the hydrophobic interaction, fucoxanthin and zeaxanthin are among the xanthophylls which bind differently by forming hydrogen bonds at Gln15A and Ser26A residues, respectively. Moreover, zeaxanthin, a β-ring carotenoid, has one hydroxyl group at each β-ionone ring. One of these hydroxyl groups interacted with the Ser26A amino acid of $A\beta_{42}$ fibril.

The formation of hydrogen bonds between donepezil, fucoxanthin, and zeaxanthin with non-amyloidic sites of Aβ has been associated with disruption and disaggregation of the beta-sheet fibril structure [52]. Not to mention, the interaction between fucoxanthin and the $A\beta_{42}$ peptide (PDB ID: 1Z0Q) prevented the conformational transition and self-

assembly of the $A\beta_{42}$ peptide [22]. The structure and conformation of carotenoids poses within different binding sites, are crucial mode by which they inhibit the formation of amyloid fibrils. The polyene backbone in carotenoids inhibits the formation of Aβ fibrils through hydrophobic interactions.

Lutein, violaxanthin, and zeaxanthin interacted with His13, while fucoxanthin interacted with His14-Gln15 residues. Meanwhile, canthaxanthin, alpha-carotene, and beta-cryptoxanthin interacted with His13-His14, Val12-His13, and Val12-His14 residues of $A\beta_{42}$ fibril, respectively. We also noticed possible interactions of alpha-carotene, astaxanthin, and canthaxanthin with Phe4 and Tyr10. Alpha-carotene and astaxanthin also interacted with His6. These carotenoids formed interactions with the $A\beta_{42}$ fibril at the S8-H14 region of amino acid, which are crucial for aggregation through interactions with metal-binding [52]. This region is also located at the N-terminus of Aβ (D1-K16), which is known to coordinate with several metal ions, including copper, zinc, and iron [53, 54].

Furthermore, lutein, violaxanthin, fucoxanthin, beta-cryptoxanthin, zeaxanthin, alpha-carotene, astaxanthin, and canthaxanthin can interact with polar residues such as His6, Tyr10, His13, His14, Gln15, and Ser26, which indicate that they have a potential for disrupting hydrogen bond formation within the Aβ peptide [55]. Apart from that, lutein and fucoxanthin also interacted with Leu17, whereas beta-cryptoxanthin interacted with amino acids Val18, Phe20, and Val24. Moreover, beta-carotene interacted with both Leu17 and Phe19 residues. These results show that lutein, violaxanthin, fucoxanthin, and zeaxanthin have the potential to inhibit the formation of $A\beta_{42}$ fibril through their interactions with F19–F20 and V24 residues. The amino acids F20-K28 of the Aβ peptide are also essential for oligomerization. These compounds inhibit Aβ aggregation by interacting with residues in the regions of S8–H14 [52-54] and K16–F20 [21]. In particular, the two aggregation-prone regions (V18-V24 and A30-V36) are also critical for the aggregation of Aβ fibrils [55]. Lutein, violaxanthin, and zeaxanthin interacted with Ala30 via hydrophobic interactions. On the other hand, lutein and violaxanthin interacted with Ile32, while fucoxanthin and beta-carotene interacted with both Ile32 and Leu34. These carotenoids can also disaggregate Aβ fibrils by interacting with the G33–G37 regions that are required for the fibrillation process [56].

Lakey-Beitia and coworkers reported that carotenoids (lutein, cryptocapsin, astaxanthin, and fucoxanthin) and apocarotenoids (bixin) could disrupt Aβ fibril by inhibiting aggregation and disaggregation pathways. Moreover, they also formed π-alkyl interactions with the S8-H14 region, which is crucial for aggregation through the interactions with metals by interacting with either both or one of these two residues, His13 and His14. The intermolecular interactions between these carotenoids with Phe19, Phe20, Val24, Ala30, and Ala32 can inhibit the aggregation and distort the S-shaped conformation of $A\beta_{42}$ fibril. However, the mechanisms for both pathways are quite different [44]. In the case of stable fibrils, the aggregation can be prevented by capping the S8-H14, K16-F20, and A21-K28 regions, which are responsible for the initiation of aggregation [21]. At the same time, the disaggregation and destabilization of Aβ fibrils can be done by interacting with residues within non-amyloidic regions [44], fibrillar axis, glycine grooves, and breaking the salt-bridges in between chains [45].

CONCLUSION

In this study, molecular docking simulations were utilized to investigate carotenoids' binding affinity and interactions derived from *Chlorella* sp. with S-shaped $A\beta_{42}$ fibril 2NAO at atomic details. The results reveal that the binding interactions were dominated by hydrophobic interaction due to the carotenoids' hydrophobicity structure, where their positions were majorly on hydrophobic residues of $A\beta_{42}$ fibril. The results also reveal that all carotenoids could potentially disrupt $A\beta_{42}$ fibril by inhibiting the aggregation pathway by interacting and capping the K16-F20 and S8-H14 regions. Their position on these two regions and their long polyene structure can prevent the new fibril from stacking to the already-formed fibril. Furthermore, five carotenoids bound to site A also can disrupt the intramolecular network of $A\beta_{42}$ fibril by interacting with Phe19, Phe20, Val24, Ala30, and Ala32 which are important residues in maintaining S-shaped $A\beta_{42}$ fibril.

ACKNOWLEDGEMENTS

The authors gratefully acknowledge financial support from the Graduate Research Fellowship (GRF) and GP-IPM Vote Number: 9628900 from Universiti Putra Malaysia (UPM) to support this work.

REFERENCES

1. Sharma, P., Sharma, A., Fayaz, F., Wakode, S. and Potto, H. F. (2020) Biological Signatures of Alzheimer's Disease. *Curr Top Med Chem*, **20(9)**, 770−781.

2. Lane, C. A., Hardy, J. and Schott, J. M. (2017) Alzheimer's disease. *European Journal of Neurology*, **25(1)**, 59−70.

3. Sochoka, M., Zwolińska, K. and Leszek, J. (2017) The Infectious Etiology of Alzheimer's Disease. *Curr Neuropharmacol*, **15(7)**, 996−1009.

4. Hardy, J. A. and Higgins, G. A. (1992) Alzheimer's Disease: the Amyloid Cascade Hypothesis. *Science*, **256(5054)**, 184−185.

5. Rosenman, D. J., Connors, C. R., Chen, W., Wang, C. Y. and Garcia, A. E. (2013) A beta Monomers

Transiently Sample Oligomer and Fibril-Like Configurations: Ensemble Characterization Using a Combined MD/NMR Approach. *J. Mol. Biol.*, **425(18)**, 3338−3359.

6. Santoro, A., Grimaldi, M., Buonocore, M., Stillitano, I., Gloria, A., Santin, M., Bobba, F., Saponetti, M. S., Ciaglia, E. and D'Ursi, A. M. (2022) New Aβ(1–42) ligands from anti-amyloid antibodies: Design, synthesis, and structural interaction. *European Journal of Medicinal Chemistry*, **237 (2022)**, 114400.

7. Mattson, M. P. (1997) Cellular actions of beta-amyloid precursor protein and its soluble and fibrillogenic derivatives. *Physiol. Rev*, **77(4)**, 1081−1132.

8. Geula, C., Wu, C. K., Saroff, D., Lorenzo, A., Yuan, M. L. and Yankner, B. A. (1998) Aging renders the brain vulnerable to amyloid beta-protein neurotoxicity. *Nature Med*, **4(7)**, 827−831.

9. McKee, A. C., Kowall, N. W., Schumacher, J. S. and Beal, M. F. (1998) Molecular Mechanisms of Neurodegenerative Diseases, Amyloid: Int. J. Exp. Clin. Invest., United Kingdom.

10. Bakare, O. O., Fadaka, A. O., Akanbi, M. O., Akinyede, K. A., Klein, A. and Keyster, M. (2021) Evaluation of selected carotenoids of Lycopersicon esculentum variants as therapeutic targets for 'Alzheimer's disease: an in silico approach. *BMC Molecular and Cell Biology*, **22**, 49.

11. Acharya, A., Stockman, J., Beyer, L., Rudack, T., Nabers, A., Gumbart, J. C., Gerwert, K., and Batista, V. S. (2020) The Effect of (-)-Epigallocatechin-3-Gallate on the Amyloid-β Secondary Structure. *Biophys J*, **119(2)**, 349−359.

12. Katarzyna, L., Sai, G., and Singh, O. A. (2015) Non-enclosure methods for non-suspended micro-algae cultivation: literature review and research needs. *Renew. Sust. Energ. Rev.*, **42(2015)**, 1418–1427.

13. Tomaselli, L. (2004) Handbook of Microalgal Culture: Biotechnology and Applied Phycology, Oxford Blackwell, United Kingdom.

14. Mata, T. M., Martins, A. A., and Caetano, N. S. (2010) Microalgae for biodiesel production and other applications: a review. *Renew. Sust. Energ. Rev.*, **14(2010)**, 217–232.

15. Nigam, P. S. and Singh, A. (2011) Production of liquid biofuels from renewable resources. *Prog. Energ. Combust. Sci.*, **37(2010)**, 52–68.

16. Priyadarshani, I. and Rath, B. (2012) Commercial and industrial applications of micro algae: a review. *J. Algal Biomass*, **3(2012)**, 89–100.

17. Yuan, X., Chen, H., Wang, Y., Schneider, J. A., Willett, W. C. and Morris, M. C. (2021) Alzheimer dementia (AD) and brain AD neuropathology: a community-based cohort of older adults. *Am. J. Clin. Nutr.*, **113(1)**, 200−208.

18. Bhattacharjee, A., Ramakrishna, A. and Obulesu, M. (2020) Phytomedicine and Alzheimer's Disease, CRC Press., Boca Raton.

19. Grodzicki, W. and Dziendzikowska, K. (2020) The Role of Selected Bioactive Compounds in the Prevention of Alzheimer's Disease. *Anti-oxidants*, **9(3)**, 229.

20. Katayama, S., Ogawa, H. and Nakamura, S. (2011) Apricot carotenoids possess potent anti-amyloi-dogenic activity in vitro. *J. Agric. Food Chem.*, **59 (2011)**, 12691–12696.

21. Lakey-Beitia, J., Kumar, D. J., Hegde, M. L. and Rao, K. S. (2019) Carotenoids as Novel Therapeutic Molecules Against Neurodegenerative Disorders: Chemistry and Molecular Docking Analysis. *Int J Mol Sci*, **20(22)**, 5553.

22. Xiang, S., Liu, F., Lin, J., Chen, H., Huang, C., Chen, L., Zhou, Y., Ye, L., Zhang, K., Jin, J., Zhen, J., Wang, C., He, S., Wang, Q., Cui, W. and Zhang, J. (2017) Fucoxanthin Inhibits β-Amyloid Assembly and Attenuates β-Amyloid Oligomer-Induced Cognitive Impairments. *J Agric Food Chem.*, **65(20)**, 4092−4102.

23. Obolesu, M., Dowlathabad, M. R. and Bramhachari (2011) Carotenoids and Alzheimer's Disease: An insight into therapeutic role of retinoids in animal models. *Neurochemistry International*, **59(5)**, 535−541.

24. Papandreou, M. A., Kanakis, C. D., Polissiou, M. G., Efthimiopoulos, S., Cordopatis, P., Margarity, M. and Lamari, F. N. (2006) Inhibitory activity on amyloid-beta aggregation and antioxidant properties of Crocus sativus stigmas extract and its crocin constituents. *J Agric Food Chem.*, **54(23)**, 8762−8768.

25. Mohammadzadeh Honarvar, N., Saedisomeolia, A., Abdolahi, M., Shayeganrad, A., Taheri Sangsari, G., Hassanzadeh Rad, B. and Muench, G. (2016) Molecular Anti-inflammatory Mechanisms of Retinoids and Carotenoids in Alzheimer's Disease: a Review of Current Evidence. *J Mol Neurosci.*, **61(3)**, 289−304.

26. Chang, C. H., Chen, C. Y., Chiou, J. Y., Peng, R. Y. and Peng, C. H. (2010) Astaxanthine secured apoptotic death of PC12 cells induced by β-amyloid peptide 25–35: its molecular action targets. *J Med Food*, **13(3)**, 548−556.

27. Sachdeva, A. K. and Chopra, K. (2015) Lycopene abrogates Aβ(1-42)-mediated neuroinflammatory cascade in an experimental model of Alzheimer's disease. *J Nutr Biochem.*, **26(7)**, 736−744.

28. Grasso, G., Rebella, M., Morbiducci, U., Tuszynski, J. A., Danani, A. and Deriu, M. A. (2019) The Role of Structural Polymorphism in Driving the Mechanical Performance of the Alzheimer's Beta Amyloid Fibrils. Front. Bioeng. *Biotechnol.*, **2019(7)**, 2296−4185.

29. Kaur, A., Kaur, A., Goyal, D. and Goyal, B. (2020) How Does the Mono-Triazole Derivative Modulate $A\beta_{42}$ Aggregation and Disrupt a Protofibril Structure: Insights from Molecular Dynamics Simulations. *ACS Omega*, **5(25)**, 15606−15619.

30. Shuaib, S., Saini, R. K., Goyal, D. and Goyal, B. (2017) Insights into the Inhibitory Mechanism of Dicyanovinyl-Substituted J147 Derivative against Aβ42 Aggregation and Protofibril Destabilization: A Molecular Dynamics Simulation Study. *ChemistrySelect*, **2017(2)**, 1645.

31. Saini, R. K., Shuaib, S., Goyal, D., Goyal, B. (2019) Insights into the inhibitory mechanism of a resveratrol and clioquinol hybrid against Aβ42 aggregation and protofibril destabilization: A molecular dynamics simulation study. *J Biomol Struct Dyn.*, **37(12)**, 3183−3197.

32. Muscat, S., Pallante, L., Stojceski, F., Danani, A., Grasso, G., Deriu, M. A. (2020) The Impact of Natural Compounds on S-Shaped Aβ42 Fibril: From Molecular Docking to Biophysical Characterization. *J Mol Sci.*, **21(6)**.

33. Wälti, M. A., Ravotti, F., Arai, H., Glabe, C. G., Wall, J. S., Böckmann, A., Güntert, P., Meier, B. H. and Riek, R. (2016) Atomic-resolution structure of a disease-relevant A beta (1-42) amyloid fibril. *Proc Natl Acad Sci U S A*, **113(34)**, E4976−E4984.

34. Morris, G. M., Huey, R., Lindstrom, W., Sanner, M. F., Belew, R. K., Goodsell, D. S. and Olson, A. J. (2009) Autodock4 and AutoDockTools4: automated docking with selective receptor flexiblity. *J. Computational Chemistry 2009*, **30(16)**, 2785−2791.

35. DS BIOVIA - Dassault Systèmes BIOVIA: San Diego, CA, USA, 2019.

36. Kim, S., Chen, J., Cheng, T., Gindulyte, A., He, J., He, S., Li, Q., Shoemaker, B. A., Thiessen, P. A., Yu, B., Zaslavsky, L., Zhang, J. and Bolton, E. E. (2019) PubChem in 2021: new data content and improved web interfaces. *Nucleic Acids Res.*, **49(D1)**, D1388–D1395.

37. Mayo, S. L., Olafson, B. D. and Goddard III, W. A. (1990) DREIDING: a generic force field for molecular simulations. *J. Phys. Chem.*, **1990(94)**, 8897−8909.

38. Daina, A., Michielin, O. and Zoete, V. (2017) SwissADME: a free web tool to evaluate pharmacokinetics, drug-likeness and medicinal chemistry friendliness of small molecules. *Sci Rep*, **7(2017)**, 42717.

39. Trott, O. and Olson, A. J. (2010) AutoDock Vina: improving the speed and accuracy of docking with a new scoring function, efficient optimization, and multithreading. *Journal of computational chemistry*, **31(2)**, 455−461.

40. Baxter J. (1981) Local optima avoidance in depot location. *Journal of the Operational Research Society*, **32(9)**, 815–819.

41. Schrodinger, L. L. C. (2010) The PyMOL Molecular Graphics System, Version 2.3.0.

42. Háda, M., Nagy, V., Deli, J. and Agócs, A. (2012) Hydrophilic Carotenoids: Recent Progress. *Molecules*, **2012(17)**, 5003−5012.

43. Bitencourt-Ferreira, G., Veit-Acosta, M. and de Azevedo, W. F. (2019) Hydrogen Bonds in Protein-Ligand Complexes. *Methods Mol Biol*, **2019(2053)**, 93−107.

44. Lakey-Beitia, J., Doens, D., Kumar, D. J., Murillo, E., Fernandez, P. L., Rao, K. S., Durrant-Archibold, A. A. (2017) Anti-amyloid aggregation activity of novel carotenoids: implications for Alzheimer's drug discovery. *Clin Interv Aging*, **2017(12)**, 815−822.

45. Kundal, K., Paramasivam, S., Mitra, A. and Sarkar, N. (2022) In silico identification of novel peptides as potential modulators of Aβ42 Amyloidogenesis. *bioRxiv*, 2022.04.20, 488983.

46. Windsor, P. K., Plassmeyer, S. P., Mattock, D. S., Bradfield, J. C., Choi, E. Y., Miller III, B. R., Han, B. H. (2021) Biflavonoid Induced Disruption of Hydrogen Bonds Leads to Amyloid-β Disaggregation. *Int. J. Mol. Sci.*, **22(6)**, 2888.

47. Lemkul, J. A. and Bevan, D. R. (2010) Destabilizing Alzheimer's Abeta(42) protofibrils with morin:

mechanistic insights from molecular dynamics simulations. *Biochemistry*, **49(18)**, 3935−3946.

48. Fan, H. M., Gu, R. X., Wang, Y. J., Pi, Y. L., Zhang, Y. H., Xu, Q., Wei, D. Q. (2015) Destabilization of Alzheimer's Aβ42 Protofibrils with a Novel Drug Candidate wgx-50 by Molecular Dynamics Simulations. *J Phys Chem B.*, **119(34)**, 11196−11202.

49. Villalobos Acosta, D. M. Á., Chimal Vega, B., Correa Basurto, J., Fragoso Morales, L. G. and Rosales Hernández, M. C. (2018) Recent Advances by In Silico and In Vitro Studies of Amyloid-β 1-42 Fibril Depicted a S-Shape Conformation. *Int J Mol Sci.*, **19(8)**, 2415.

50. Xiao, Y., Ma, B., McElheny, D., Parthasarathy, S., Long, F., Hoshi, M., Nussinov, R. and Ishii, Y. (2015) Aβ(1-42) fibril structure illuminates self-recognition and replication of amyloid in Alzheimer's disease. *Nat Struct Mol Biol.*, **22(6)**, 499−505.

51. Garbuzynskiv, S. O., Lobanov, M. Y. and Galzitskaya, O. V. (2010) Fold Amyloid: a method of prediction of amyloidogenic regions from protein sequence. *Bioinformatics*, **26(3)**, 326–332.

52. Hetényi, C., Körtvélyesi, T. and Penke, B. (2002) Mapping of possible binding sequences of two beta-sheet breaker peptides on beta amyloid peptide of Alzheimer's disease. *Bioorg Med Chem.*, **10(5)**, 1587–1593.

53. Kepp, K. P. (2017) Alzheimer's disease: How metal ions define β-amyloid function. *Coord. Chem. Rev.*, **351**, 127–159.

54. Lin, T. W., Chang, C. F., Chang, Y. J., Liao, Y. H., Yu, H. M. and Chen, Y. R. (2017) Alzheimer's amyloid-β A2T variant and its N-terminal peptides inhibit amyloid-β fibrillization and rescue the induced cytotoxicity. *PLoS ONE*, **12(3)**, e0174561.

55. Cheon, M., Hall, C. K. and Chang, I. (2015) Structural Conversion of Aβ17–42 Peptides from Disordered Oligomers to U-Shape Protofilaments via Multiple Kinetic Pathways. *PLoS Comput Biol.*, **11(5)**, e1004258.

56. Lakey-Beitia, J., Jagadeesh Kumar, D., Muralidhar, L. Hegde. and Rao, K. S. (2019) Carotenoids as Novel Therapeutic Molecules Against Neurodegenerative Disorders: Chemistry and Molecular Docking Analysis. *Int. J. Mol. Sci.*, **20**, 5553.